https://doi.org/10.18485/resylab.2024.6.ch12 PROCEEDINGS PAPER

Interpretation challenges when detecting landslides in flysch environment: examples from visual analysis of LiDAR DTM in the City of Buzet

Petra Jagodnik[(1)*], Sanja Bernat Gazibara[(2)], Federica Fiorucci[(3)], Michele Santangelo[(3)]

1) University of Rijeka, Faculty of Civil Engineering, Rijeka, Radmile Matejčić 3, Croatia, +38551265959 (petra.jagodnik@gradri.uniri.hr)

2) University of Zagreb, Faculty of Mining, Geology and Petroleum Engineering, Zagreb, Croatia

3) Research Institute for Geo-Hydrological Protection, Perugia, Italy

Abstract This paper presents examples of interpretation challenges in unambiguous landslide detection arising from the visual interpretation of 0.3 m LiDAR DTM in the City of Buzet (20 km²), Croatia. The study area is within the Istrian Flysch, for which the large-scale geomorphological landslide inventory mapping was performed for the first time. First, we present distinctive concave forms detected along the hillslopes and discuss whether they represent landslides or not. Furthermore, we present examples of the geomorphological convergence between the landslides and erosional features formed along gully channel walls. Finally, we show examples of Badlands topography on LiDAR DTM derivatives and point to the similarity of these phenomena with landslide features.

Keywords landslide detection, visual interpretation, LiDAR DTM, geomorphological convergence, landslides in flysch, City of Buzet

Introduction

Landslide inventory maps document the extent of landslides in a territory, providing information about the spatial distribution, types, pattern, recurrence and statistics of landslides (Guzzetti et al. 2012). Inventory maps are commonly prepared by the visual interpretation of LiDAR (Light Detection and Ranging) Digital Terrain Model (DTM) morphometric derivatives (Scaioni et al. 2014), especially in area covered by dense forests (e.g., Ardizzone et al. 2007; Van den Eeckhaut et al. 2007; Razak et al. 2011), by detecting the geomorphic expression of landslide features (Soeters and van Westen 1996). Given that landslide inventories are essential input data for subsequent analyses in landslide research, e.g., landscape evolution (Guzzetti et al. 2008; Bibentyo et al. 2024) or susceptibility modelling (van Westen et al. 2006), the quality of the landslide map, controlled by its accuracy and certainty of the presented information, is a critical issue. Accuracy of a landslide inventory depends on geographical and thematic correctness of the information shown on the map, as well as on its completeness, i.e. the proportion of mapped landslides compared to the ground truth (Guzzetti et al. 2012). While geographic accuracy depends on the type and resolution of the interpreted imagery, completeness of the landslide map may strongly vary due to the interpreter's skills and experience at detection and classification of slope failures.

Distinguishing landslides from other specific geomorphic expressions becomes challenging task even for highly experienced interpreters when mapping is carried out in geologically complex settings, especially if an area is affected by multiple geomorphological processes. In that case, errors in landslide detection may arise either from geomorphologic convergence between landslides and other geological processes (Hart et al. 2012) and certain surface deposits (Antonini et al. 2002), or if the landslide topography has been dismantled (Jagodnik et al. 2020). In terrains characterized by mechanically weak lithology, e.g., siliciclastic rocks, weathering processes and high erodibility of bedrock favor the superimposition of the signature of various denudational forms (Ciccacci et al. 2008).

Most of the landslide research based on the visual interpretation of LiDAR DTM commonly present examples of the typical landslide topography identified on DTM derivatives (e.g. Petschko et al. 2015; Görum 2019). On the other hand, there is a lack of studies focusing on the interpretation difficulties in landslide mapping on LiDAR DTM derivatives. In this paper we present and discuss the challenges in landslide detection and mapping specific for the flysch environment, based on the experience of the visual interpretation of 0.3 m LiDAR DTM in the City of Buzet (Bernat Gazibara et al. 2023; Jagodnik et al. 2023). The study area is terrain in Istrian Flysch, composed of a rhythmical alternation of hemipelagic marls and turbidities (Marinčić et al. 1996). Although landslides frequently occur in the Istrian Flysch (Arbanas et al. 2014), no systematic landslide inventory mapping has been carried out so far. The research was conducted within the frame of scientific research project "Methodology development for landslide susceptibility assessment for land-use planning based on LiDAR technology" (LandSlidePlan, HRZZ IP-2019-04-9900).

Study area

The study area (20 km²) is in the northern Istria, in Croatia. It is the part of the City of Buzet, between the Mirna River Valley in the north and the Butoniga water reservoir in the south (Fig. 1). The terrain predominantly consists of Middle Eocene clastic sedimentary rocks (Fig. 1a), also

known as Istrian Flysch, super-positioned on the Palaeogene *Globigerina* marls, and foraminiferal limestone (Pleničar et al. 1969). Flysch deposits can be stratigraphically divided into the lower and upper units (Marinčić et al. 1996; Bergant et al. 2003). The lower flysch unit is composed of a rhythmical alternation of marls and carbonates (i.e. breccias, conglomerates and bioclastic arenites), while in the upper flysch unit thin layers of carbonate-siliciclastic turbidity sediments are deposited. According to Petrinjak et al. (2021), carbonate megabeds composed of lithoclasts from the underlying limestone can be found in different stratigraphic positions within the flysch succession. The estimated total thickness of Istrian Flysch is 350 m.

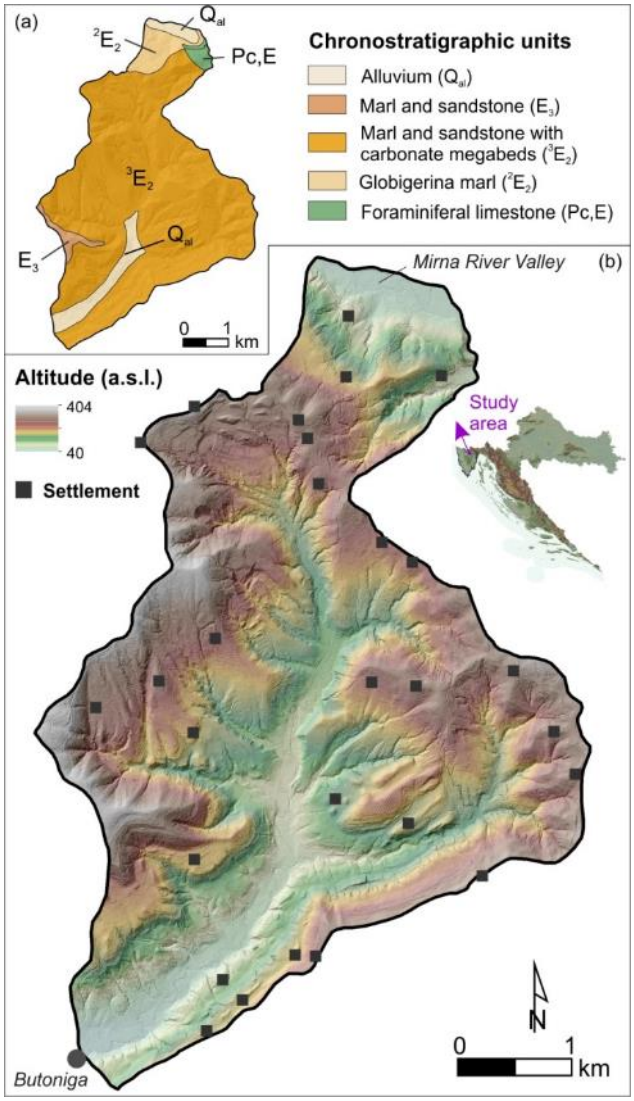

Figure 1 Study area in the City of Buzet: (a) simplified geologic map (after Pleničar et al. 1969); and (b) relief map.

The relief is hilly and moderately dissected (Fig. 1b). Predominant slope angles range from 13° to 32°. Prevailing elevations range from 100 to 300 m a.s.l.. Approximately 55% of the area is covered by forests, while ~40% is an agricultural area (Sinčić et al. 2022). The climate is temperate with hot summers, the coldest months averaging 0°C, and no dry season. Mean annual precipitation is 1,200-1,300 mm (Zaninović et al. 2008).

Due to low durability of flysch bedrock (Gulam et al. 2018) and intensive weathering processes (Vivoda Prodan et al. 2017), slopes are typically covered by Quaternary superficial deposits (Dugonjić Jovančević and Arbanas 2012). There is an interplay between mass movements and linear erosion, resulting in numerous active landslides (Arbanas et al. 2014), gullies (Jagodnik et al. 2023), and Badlands (Gulam et al. 2014; Bostjančić et al. 2023). So far, more than 1,100 landslides have been identified in the study area (Jagodnik et al. 2023), and the landslide inventory mapping is still in progress. Landslides mostly occur in gullies and low-order valleys, as well as on terraced hillslopes and slope segments with concentrated surface runoff, e.g. near roads. They are predominantly small to medium-sized debris slides and earth slides, caused by rainfall and/or human activity (Arbanas et al 2007). Sliding mostly occur along the contacts between superficial deposits and bedrock, or within the weathered flysch (Dugonjić Jovančević and Arbanas 2012). Deep seated landslides were also identified; with certain phenomena being large, very old and relict (Jagodnik et al. 2023).

Landslide inventory map

LiDAR datasets

The LiDAR data used in this study were acquired in the framework of the LandSlidePlan scientific project. Airborne laser scanning was performed in March 2020, at an average altitude of 700 m a.s.l., with an average point density of 16,09 pt./m², thus resulting in average point spacing of 0.18 cm. The classified Point Cloud ground bare-earth points were interpolated using kriging interpolation method, and the DTM was generated at a spatial resolution of 0.3 m.

Visual interpretation of LiDAR DTM derivatives

For the landslide detection and mapping, the following morphometric datasets were derived from the DTM: (i) hillshade maps, using the sun azimuth angles 315° and 45°, and the sun elevation angles of 45°; (ii) slope map; (iii) and contour line maps, created with 1-m; 2-m; and 5-m contour intervals. Additional topographic information was available from two official state maps: (i) the digital orthophoto (DOF) from year 2020, at a resolution of 0.5 m; and (ii) the Croatian Base Map (CBM) at a scale of 1:5,000.

In general, landslide detection relies on the identification of a set of photographic/radiometric and morphologic evidence that characterizes an anomaly within the lateral continuity of the other landscape features (e.g., the morphological trace of bedding, scarps; Santangelo et al., 2022). Landslide identification on LiDAR DTM data relies on a reduced set of evidence, as no radiometric information is available, which increases the level of uncertainty. On the other hand, the use of DTM derivatives may help enforcing the set of evidence to detect and map landslides. Figure 2 shows an example of evidence collected on a slope where the lateral continuity of extended linear features is suddenly interrupted by an area characterized by a concave-convex topographic profile, a coarser texture, and a larger scale roughness compared to the surrounding area. All these elements converge towards the identification of a landslide with little uncertainty. In cases where such set of evidence is poorer, uncertainty is higher. It must be stated here that collecting such elements is not only a matter of the images portraying the landslide features, but also a matter of the capability and experience of the interpreter to spot them and relate them to produce a sort of multivariate expert model in their mind.

In this phase of landslide inventory mapping, two levels of confidence of interpretation were distinguished: high, and low. Thereby, the high level of confidence implies that the landslide morphological signature is obvious on DTM derivatives (Fig.3). On the other hand, the low level of confidence implies either: (i) that the landslide topography is poorly expressed on DTM derivatives; (ii) or that part of a landslide is not visible; or (iii) that the topography of the observed phenomenon is clearly expressed on DTM derivatives, but there is a doubt depending on the interpreter's experience.

In the study area, most of the challenges in the identification and mapping of landslides are related to distinguishing landslides from other similar geomorphic expression observable on LiDAR DTM derivatives. Characteristic examples are presented and discussed in the following section.

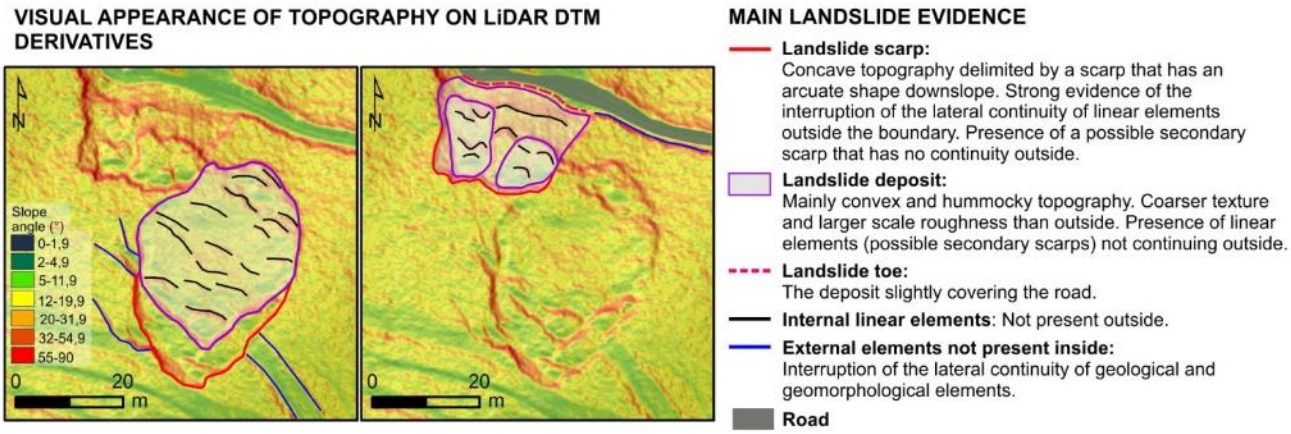

Figure 9 Example of the collection of main landslide evidence converging towards the identification of a landslide with high level of confidence. The hillshade map is overlapped by the semi-transparent (30% transparency) slope map.

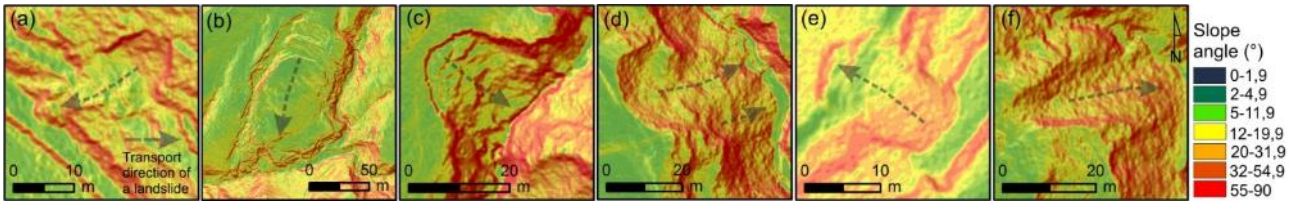

Figure 3 Examples of the landslides identified with high level of confidence in interpretation. Landslide boundaries are not presented for easier recognition of the landslide topography on LiDAR DTM derivatives. In all examples, the hillshade map is overlapped by the semi-transparent (30% transparency) slope map.

Challenges in landslide detection on LiDAR DTM: characteristic examples

Concave forms along hillslopes: landslides or not?

Figure 4a presents distinctive hillslope topography in the study area, characterized by linear features of agricultural terraces and bedding of competent flysch lithology. Most of the terraced landscape is now abandoned and covered by dense forests, thus there are favourable conditions for the land degradation (Tarolli et al. 2019). Here, numerous concave forms resembling landslide crowns and flanks are expressed on DTM derivatives. However, the anthropic elements are usually regular and rectilinear, whereas the bedding in this area appears continuous and does not show local variations both in attitude and in thickness. Landslides cause local interruption of anthropic elements and local variations in the continuity of bedding traces. In detail, the observed feature is considered a landslide (continuous red line in Fig. 4b) if the disturbance of linear hillslope element is evident, together with the evidence of distinctive toe topography. Other morphologies similar to landslide crowns and flanks are uncertain to be landslides (presented by red dashed line in Fig. 4b), especially if associated with persistent bedding (pointed by black arrows in Fig. 4b). Moreover, landslide accumulation zones in such cases were usually not detected. Such phenomena could be considered to represent evidences of erosional fluting formed at slope segments with concentrated runoff along the structural discontinuities.

Morphological features similar to landslide crowns (presented by blue dashed line in Fig. 4b) were also detected around gullies, which often form on the hillslopes near roads. Although they can easily be misinterpreted as landslides, they actually represent features of the gully head. In the study area, there are numerous similar morphological expressions observed, especially around the soft gully margins (Brooks et al. 2019) of more complex and older gully systems.

Concave scarps in gullies

Figure 5 presents examples of landslide identification within gullies. More than 300 gullies of different types and evolution states are identified in the study area, comprising more than a half of the total number of identified landslides (Jagodnik et al. 2023). The most challenging identification of landslides was precisely within gully landforms, since there are distinctive morphologies that share little apparent difference between each other on LiDAR DTM derivatives but have been formed by different geomorphological processes.

Many landslides in gullies are interpreted with high level of confidence if their features are preserved and clearly expressed on DTM derivatives (Fig. 5a). The landslide mapping was also facilitated by the fact that the landslide crown usually coincides with the gully edge, while the landslide toe reaches the gully thalweg (Jagodnik et al. 2020). However, many gullies in the study area have a specific appearance on DTM derivatives (Fig. 5b) with numerous ridges and concavities that appear like zones of landslide crowns and depletion (pointed by blue arrows in Fig. 5d). The DOF analysis (Fig. 5c) indicated that such gullies have characteristics of the B-type calanchi landforms (Rodolfi and Frascati 1979). Landslides within them were delineated only in the cases when all features were detected on DTM derivatives (Fig. 5d), but the level of interpretation confidence is often low

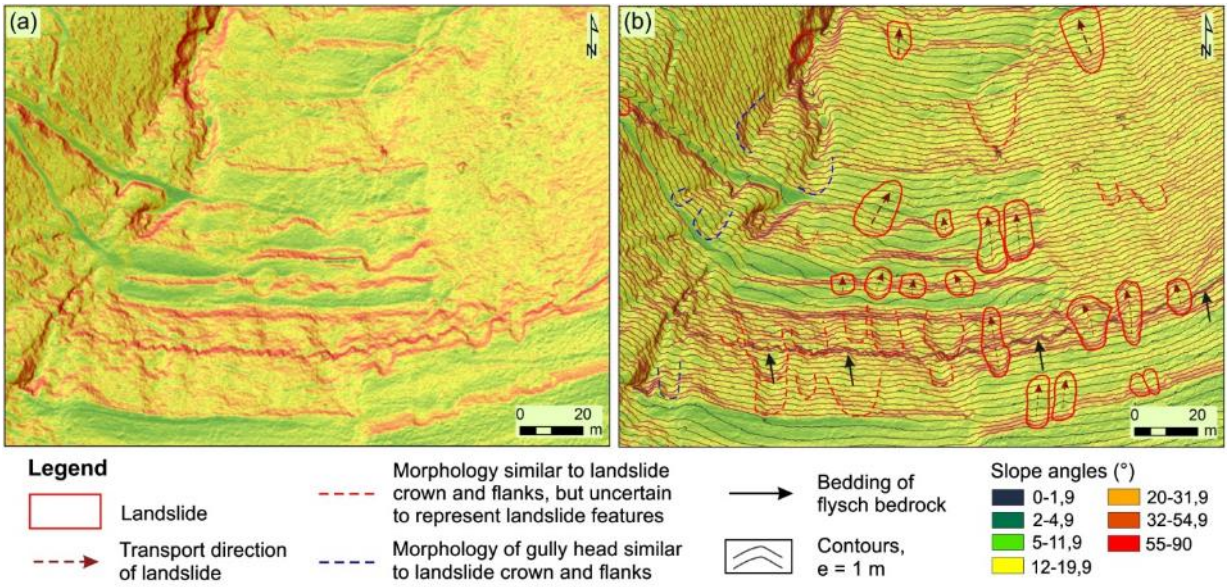

Figure 4 Example of the distinctive topography of flysch hillslopes in the study area, with landslides and concave forms resembling landslide features: (a) without, and (b) with interpretation. The hillshade map is overlapped by the semi-transparent (30%) slope map.

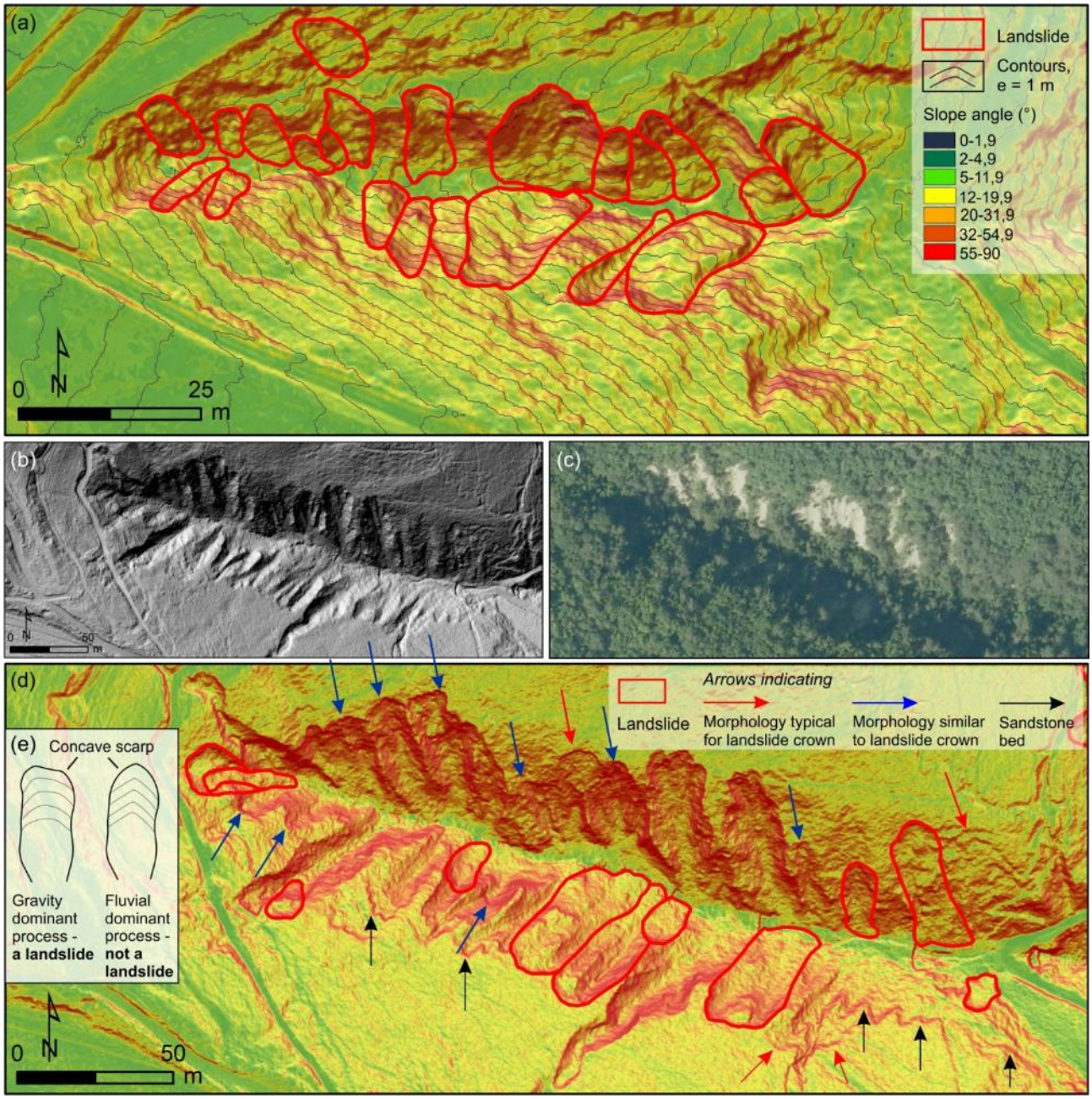

Figure 5 Identification and mapping of landslides within gullies: (a) examples of landslides identified with high level of confidence; (b) example of distinctive topography of gully landforms having characteristics of the B-type calanchi (Rodolfi and Frascati 1979) on the hillshade map; and (c) on the digital ortophoto (DOF); (d) examples of geomorphological convergence between the morphologies typical for landslide crowns and erosional concave scars, with identified landslides; and (e) the pattern of contour lines reflecting the dominant formative process of a concave phenomenon.

On the opposite, where only the concave scars are expressed but not the landslide deposit, care must be taken not to misinterpret them as landslides. Still, there is a doubt as to whether some of these phenomena are traces of debris flows formed along gully walls, with toes being removed by the active gully erosion. For a more reliable distinguishing of the dominant process forming similar phenomena, more detailed analysis of the pattern of contour lines reflecting the shape of a concave scarp should be performed (Fig. 5e).

Badland or landslide phenomenon?

Figure 6 presents examples of the valley topography associated to badlands and landslide occurrences in the study area, as well as the example when a badland phenomenon was initially misinterpreted as a landslide. Clearly observable landslides, identified with high confidence, are pointed by red arrows in Fig. 6d.

During the preliminary visual analysis of the hillshade map (Fig. 6a), topographic contour lines on CBM (Fig. 6b), and DOF (Fig. 6c), the phenomenon marked by number 1 was first identified as a landslide with a small

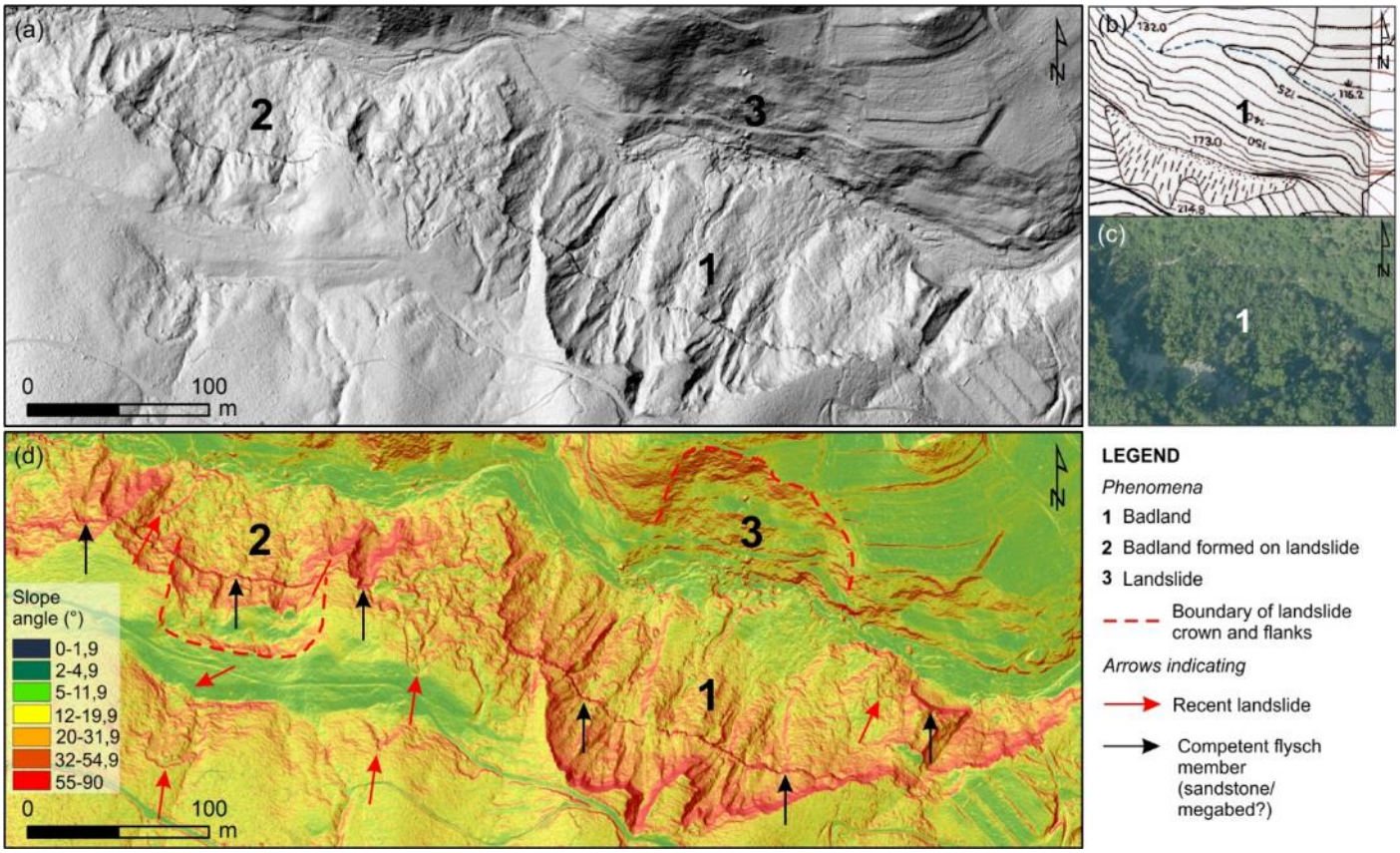

Figure 6 Example of the topography associated to Badlands and landslides: (a) appearance of the observed phenomena marked by numbers 1, 2, and 3 on the hillshade map; (b) appearance of the phenomenon marked by number 1 on the Croatian Base Map (CBM) 1:5,000; and (c) on the DOF; appearance of the observed phenomena marked by numbers 1, 2, and 3 on the slope map, with points to recent landslides and bedding of flysch bedrock.

badland formed within the depletion zone. The landslide was primarily assumed by the arcuate shape and steep slope angles distributed along the head segment visible on the slope map (Fig. 5d), as well as the sharp flanks, and the accumulated material that pushed the watercourse at the foot slope. However, a more detailed analysis of other topographic features, especially the linear features of bedding persistence of competent flysch members (pointed by black arrows in Fig. 5d), identified the phenomenon as the A/B-type of badland (Rodolfi and Frascati 1979), having a typical horse-shoe appearance with sharp edges still present, and the valley bottom filled by earth-flow deposits covered by vegetation. Several small recent landslides are identified along the surface of the badland phenomenon 1.

Similar badland topography was also observed in the case of the phenomenon marked with number 2, which was formed along the body of an older landslide. A deep-seated landslide, acting as the host phenomenon of the badland formation, is indicated by the topography specific for landslide crown, main scarp, and head visible on the slope map (dashed red line in Fig. 5d). The topography of adjacent deep-seated landslide identified in the presented environment is marked by number 3 in the figure.

Conclusions

Based on the experience in the visual interpretation of 0.3 m LiDAR DTM of the study area in the City of Buzet in Istria (Croatia), and the presented examples, we conclude that the difficulties in landslide detection in flysch environment mostly arise from their similarity to erosional forms. The most challenging was to distinguish the topography of particular landslide features, i.e. crowns and flanks from numerous concave scars formed by linear erosion along gully channel walls. Yet, many landslides within certain gullies have been identified with high level of confidence, in the cases when all landslide features could have been detected on LiDAR DTM derivatives. In order to more reliably distinguish the landslides from morphologically similar erosional forms, a detail analysis of the pattern of contours reflecting the shape of a concave form is recommended. In general, using a wide and rigorous set of evidence, and a reproducible procedure to detect landslides is essential, as it limits both omission and commission errors, positively impacting the completeness, i.e., statistical representativeness of the final inventory and, hence, its quality.

Acknowledgements

This research was funded by the Croatian Science Foundation under the project Methodology development for landslide susceptibility assessment for land-use planning based on LiDAR technology (HRZZ IP-2019-04-9900, HRZZ DOK-2020-01-2432). It was partially supported by the project of the University of Rijeka Landslides and erosion as associated geological hazards in flysch environment (uniri-iskusni-tehnic-23-191). These supports are gratefully acknowledged.

References

Antonini G, Ardizzone F, Cardinali M, Galli M, Guzzetti F, Reichenbach P, (2002) Surface deposits and landslide inventory map of the area affected by the 1997 Umbria–Marche earthquakes. Bollettino della Societa Geologica Italiana. 121(2): 843–853.

Arbanas Ž, Grošić M, Goršić D, Griparić B, (2007) Landslides remedial works on small roads of Istria. Proceedings of the 4th Croatian Roads Congress. p.38.

Arbanas Ž, Jovančević S D, Vivoda M, Mihalić Arbanas S, (2014) Study of Landslides in Flysch Deposits of North Istria, Croatia: Landslide Data Collection and Recent Landslide Occurrences. Landslide Science for a Safer Geoenvironment. Springer International Publishing, Cham. pp. 89-94.

Ardizzone F, Cardinali M, Galli M, Guzzetti F, Reichenbach, P (2007) Identification and mapping of recent rainfall-induced landslides using elevation data collected by airborne LiDAR. Natural Hazards and Earth System Sciences. 7(6): 637–650.

Bergant S, Tišljar J, Šparica M, (2003) Eocene carbonates and flysch deposits of the Pazin Basin. Field trip guidebook of 22nd IAS meeting of sedimentology, 17-19 September 2003. Opatija, Croatia. pp. 57-63.

Bernat Gazibara S, Jagodnik, P, Lukačić, H, et al., (2023) Landslide and soil erosion inventory mapping based on high-resolution remote sensing data: a case study from Istria (Croatia). Progress in Landslide Research and Technology, Vol. 2. Springer International Publishing, Cham. pp. 363-375.

Bibentyo T M, Dille A, Depicker, A, et al., (2024) Landslides, bedrock incision and human-induced environmental changes in an extremely rapidly formed tropical river gorge. Geomorphology. 449: 109046.

Bostjančić I, Gulam V, Frangen T, Hećej N, (2023) Relation between relief and Badland spatial distribution in the Paleogene Pazin Basin, Croatia. Journal of Maps. 19:1: 2163196.

Brooks A, Thwaites R, Spencer J, Pietsch T, Daley, J (2019) A Gully Classification Scheme to Underpin Great Barrier Reef Water Quality Management: 1st Edition. Report to the National Environmental Science Program. Reef and Rainforest Research Centre Limited, Cairns. 123 pp.

Ciccacci S, Galiano M, Roma M A, Salvatore, M C, (2008) Morphological analysis and erosion rate evaluation in badlands of Radicofani area (Southern Tuscany – Italy). Catena. 74: 87-97.

Dugonjić Jovančević S, Arbanas Ž, (2012) Recent Landslides on the Istrian peninsula, Croatia. Natural Hazards. 62:1323-1338.

Görum T, (2019) Landslide recognition and mapping in a mixed forest environment from airborne LiDAR data. Engineering Geology. 258, 105155.

Gulam V, Pollak D, Podolszki L, (2014) The analysis of the flysch badlands inventory in central Istria. Geologia Croatica. 67/1: 1-15.

Gulam V, Gajski D, Podolszki L, (2018) Photogrammetric measurement methods of the gully rock wall retreat in istrian badlands. Catena. 160: 298-309.

Guzzetti F, Ardizzone F, Cardinali M, Galli M, Reichenbach, P, (2008) Distribution of landslides in the Upper Tibet River basin, central Italy.Geomorphology. 96:105-122.

Guzzetti F, Mondini A C, Cardinali M, Fiorucci, F, Santangelo, M, Chang, K T, (2012) Landslide inventory maps: new tools for an old problem. Earth-Science Reviews. 112: 42-66.

Hart M W, Shaller P J, Farrand G T, (2012) When Landslides are Misinterpreted as Faults: Case Studies from the Western United States.

Jagodnik P, Jagodnik V, Arbanas Ž, Mihalić Arbanas S, (2020) Landslide types in the Slani Potok gully, Croatia. Geologia Croatica. 73/1:13-28.

Jagodnik P, Bernat Gazibara S, Sinčić M, et al. (2023) Landslides, gully erosion and badlands as associated geological hazards in flysch environment – analysis of geomorphological inventories and LiDAR DTM at a large scale. Proceedings of the 6th World Landslide Forum-Abstract Book. Florence, Italy. p. 110-110.

Marinčić S, Šparica M, Tunis G, Uchman A, (1996) The eocene flysch deposits of the Istrian peninsula in Croatia and Slovenia. Regional, stratigraphic, sedimentological and ichnological analysis. Annales. 9:139-156.

Petschko H, Bell R, Glade T, (2015) Effectiveness of visually analyzing LiDAR DTM derivatives for earth and debris slide inventory mapping for statistical susceptibility modeling. Landslides. 13(5): 857–872.

Petrinjak K, Budić M, Bergant S, Korbar, T, (2021) Megabeds in Istrian Flysch as markers of synsedimentary tectonics within the Dinaric foredeep (Croatia). Geologia Croatica. 74/2: 99-120.

Pleničar M, Polšak A, Šikić D, (1969) Osnovna geološka karta SFRJ 1:100000, list Rovinj L33-100 [Basic geological Map of SFRY 1:100000, Rovinj sheet – in Croatian]. Institut za geološka istraživanja, Zagreb; Savezni geološki zavod.

Razak K A, Straatsma M W, van Westen C J, Malet J-P, de Jong S M, (2011) Airborne laser scanning of forested landslides characterization: terrain model quality and visualization. Geomorphology. 126: 186–200.

Rodolfi G, Frascati F, (1979) Cartographia di base per la programmazione degli interventi in aree marginali (area rappresentativa della Val D'Era). Annali Ist. Per Io Studio e la Difesa del Suolo, vol. 10.

Santangelo M, Cardinali M, Bucci F, Fiorucci F, Mondini A C (2022) Exploring event landslide mapping using Sentinel-1 SAR backscatter products. Geomorphology. 397: 108021.

Scaioni M, Longoni L, Melillo V, Papini M, (2014) Remote Sensing for Landslide Investigations: An Overview of Recent Achievements and Perspectives. Remote Sensing. 6(10): 9600-9652.

Sinčić M, Bernat Gazibara S, Krkač M, Lukačić H, Mihalić Arbanas S, (2022) The Use of High-Resolution Remote Sensing Data in Preparation of Input Data for Large-Scale Landslide Hazard Assessment. Land. 11:1360.

Soeters R, van Westen C J, (1996) Slope instability recognition, analysis, and zonation. Turner, A K, Schuster, R L (eds.): Landslides, Investigation and Mitigation. Transportation Research Board, Special Report 247, Washington D.C., USA (ISBN 0-309-06151-2). 129-177.

Van den Eeckhaut M, Poesen J, Verstraeten G, Vanacker V, Nyssen J, Moeyersons J, Van Beek L P H, Vandekerckhov L, (2007) Use of LIDAR-derived images for mapping old landslides under forest. Earth Surface Processes and Landforms. 32: 754–769.

van Westen C J, van Asch T W J, Soeters R, (2006) Landslide hazard and risk zonation – why is it still so difficult? Bulletin of Engineering Geology and the Environment. 65: 167-184.

Tarolli P, Rizzo D, Brancucci G, (2019) Terraced Landscapes: Land Abandonment, Soil degradation, and Suitable Management.

World Terraced Landscapes: History, Environment, Quality of Life, Chapter 12. Springer. 195-210.

Vivoda Prodan M, Mileusnić M, Mihalić Arbanas S, Arbanas Ž, (2017) Influence of weathering processes on the shear strength of siltstones from a flysch rock mass along the northern Adriatic coast of Croatia. Bulletin of Engineering Geology and the Environment. 76/2: 695-711.

Zaninović K, Gajić-Čapka M, Perčec Tadić, M, et al., (2008) Klimatski atlas Hrvatske 1961-1990, 1971-2000 [Climate atlas of Croatia – in Croatian]. Državni hidrometeorološki zavod, Zagreb (ISBN 978-953-7526-01-6). 200p.